Capacity Analysis of Orbital Angular Momentum Wireless Channels

IEEE Access
Multidisciplinary | Rapid Review | Open Access Journal

Received September 14, 2017, accepted October 3, 2017, date of publication October 17, 2017,
date of current version November 14, 2017.

Digital Object Identifier 10.1109/ACCESS.2017.2763679

Capacity Analysis of Orbital Angular Momentum Wireless Channels

LIANG WANG[1], XIAOHU GE[1], Senior Member, IEEE, RAN ZI[1], Student Member, IEEE, AND CHENG-XIANG WANG[2], Fellow, IEEE

[1]School of Electronic Information and Communications, Huazhong University of Science and Technology, Wuhan 430074, China
[2]Institute of Sensors, Signals and Systems, School of Engineering and Physical Sciences, Heriot-Watt University, Edinburgh EH14 4AS, U.K.

Corresponding author: Xiaohu Ge (e-mail: xhge@mail.hust.edu.cn).

This work was supported in part by the NSFC Major International Joint Research Project under Grant 61210002, in part by the Fundamental Research Funds for the Central Universities under Grant 2015XJGH011, in part by the EU FP7-PEOPLE-IRSES (Project acronym CROWN), under Grant 610524, in part by the China International Joint Research Center of Green Communications and Networking under Grant 2015B01008, in part by the EU H2020 RISE TESTBED Project under Grant 734325, in part by the EU FP7 QUICK Project under Grant PIRSES-GA-2013-612652, and in part by the EPSRC TOUCAN Project under Grant EP/L020009/1.

ABSTRACT The orbital angular momentum (OAM) technology is able to provide a new degree of freedom for wireless communication systems. The energy of OAM waves is focused within a circle region surrounding the beam axis, which makes the propagation gains inside and outside the circle region different. However, in the existing literature, the propagation gains inside and outside the circle region are assumed to be the same. Therefore, the impact of OAM waves' spatial energy distribution on the capacity of OAM wireless communication systems has not been fully investigated. Considering the spatial energy distribution characteristics of OAM waves, in this paper, an OAM wireless channel model is proposed. Based on the proposed OAM wireless channel model, the capacity of OAM-based multiple-input multiple-output (MIMO) communication system is analytically derived. Simulation results indicate that the capacity of OAM-based MIMO system outperforms the capacity of conventional MIMO system when the transmission distance is larger than a specific threshold. Our results provide a basic capacity model for OAM-based MIMO communication systems.

INDEX TERMS Orbital angular momentum (OAM), wireless channel model, multiple-input multiple-output (MIMO), capacity.

I. INTRODUCTION

With the explosive growth of wireless throughput, improving wireless capacity has become one of the main goals in the future fifth generation (5G) communication systems [1]–[6]. Different multiplexing schemes, such as time division multiplexing, frequency division multiplexing and spatial division multiplexing have been widely employed to improve the wireless capacity in current wireless communication systems [7]. In addition to these conventional multiplexing schemes which utilize degrees of freedom in time, frequency and space domains, the orbital angular momentum (OAM) technology is able to provide a new degree of freedom, i.e., the OAM state for wireless communications. There exists a potentially revolutionary improvement in wireless capacity when the OAM technology is used for 5G wireless communication systems. Different from the propagation patterns of conventional electromagnetic waves, the energy of OAM waves is focused within a circle region surrounding the beam axis, which leads to different propagation gains inside and outside the circle region. Precisely modeling the capacity of OAM wireless communication systems considering propagation gain features is one of the key issues to apply the OAM technology for the 5G wireless communication systems.

It is well known that electromagnetic waves carry both linear momentum and angular momentum. The angular momentum is divided into the spin angular momentum (SAM) and the OAM. The SAM, which is associated with the polarization of electromagnetic waves, has only two orthogonal states [8]. Compared with the SAM, the OAM is associated with the spatial distribution of electromagnetic waves and has unbounded eigenstates, *i.e.*, OAM states [9]. Since Allen *et al.* recognized the light beams with the transverse azimuthal phase distribution carry the OAM [10], the

application of OAM waves has become an attractive solution for improving the communication systems' capacity [11]–[15]. In optical communications, it was demonstrated that OAM waves with different OAM states can be multiplexed to achieve the capacity of *Tbps* and high spectral efficiency [16]. In [17] the trench-assisted multi-OAM multi-ring fiber was designed to enable *Pbps* ($10^{15}bps$) total transmission capacity and hundreds bit/s/Hz spectral efficiency. Besides the OAM technology used for optical communications, the OAM technology has been explored to improve the capacity of wireless communications in microwave and millimeter wave frequencies [18]–[23]. It was shown that OAM waves can be generated by uniform circular array (UCA) and used in wireless communications [18]. The experiments in Venice demonstrated that two radio signals with different OAM states can be transmitted and received simultaneously on the same frequency [19]. Since then, the comparison between OAM wireless communication systems and other conventional wireless communication systems have been extensively studied. Considering the configuration of UCA in free space environments, Ove et al., indicated that the capacity over sub-channels given by OAM states is a subset of solutions offered by the conventional multi-input multi-output (MIMO) method [20]. Cagliero indicated that OAM systems and MIMO systems offer the same performance when the transmitting UCA and receiving UCA are on-axis, but small misalignments between the OAM transmitting and receiving arrays severely degrade the system performance [21]. The results in [22] showed that the capacity of line of sight (LoS) MIMO systems is enhanced by OAM waves when the number of receiving antennas of receiving UCA is larger than the number of transmitting antennas of transmitting UCA. In [23] an OAM-based MIMO communication system was proposed to achieve an adequate capacity when uniform linear array (ULA) with traveling-wave antennas is equipped at the transmitter.

However, in the above studies on OAM wireless communication systems, the OAM wireless channels have been assumed as the free space channels with equal gains in different propagation directions, *i.e.*, the propagation gains inside and outside the circle region have been assumed to be the same [23]. This assumption is against with the spatial energy distribution of OAM waves where the energy of OAM waves is focused within a circle region surrounding the beam axis [24]–[26]. Therefore, it is an important issue to evaluate the capacity of OAM wireless communication systems considering the spatial energy distribution characteristics of OAM waves.

Based on the spatial energy distribution characteristics of OAM waves, in this paper the OAM wireless channel is first modeled. Furthermore, the capacity of OAM-based MIMO communication system is analytically derived based on the proposed OAM channel model. Simulation results indicate that the capacity of OAM-based MIMO system outperforms the capacity of conventional MIMO system when the propagation distance is larger than a specific threshold.

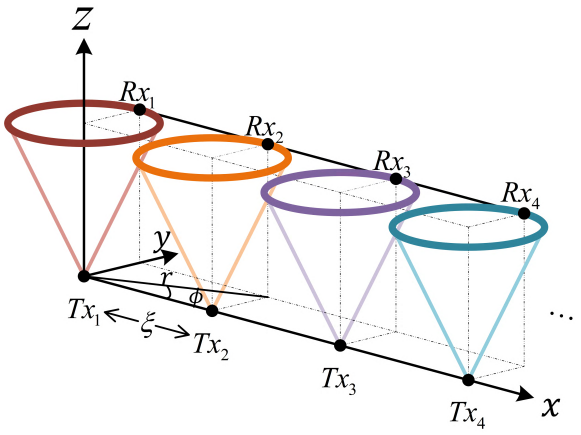

FIGURE 1. System model.

The rest of this paper is organized as follows. In Section II, the OAM-based MIMO communication system model is introduced, the OAM wireless channel is modeled, and the capacity of OAM-based MIMO communication systems is derived based on the proposed OAM wireless channel model. In Section III, simulation results are analyzed. In the end, conclusions are drawn in Section IV.

II. SYSTEM MODEL

In this section, based on the spatial energy distribution characteristics of OAM waves, an OAM-based MIMO communication system is illustrated and the OAM wireless channel is modeled. Then, the capacity of the OAM-based MIMO communication system is derived based on the proposed OAM wireless channel model.

A. OAM-BASED MIMO SCHEME

The system model is illustrated in Fig. 1. The transmitter is equipped with a ULA consisting of N transmitting antennas. The receiver is also equipped with a ULA consisting of M receiving antennas. The transmitting antennas are traveling-wave antennas equipped with carefully designed reflectors [27]–[29]. Traveling-wave antennas can generate OAM waves and sophisticated reflector can help to focus OAM waves with different OAM states and improve the directivity of radiated waves [28]. The OAM waves generated by different antennas have different OAM states, which makes OAM waves orthogonal to each other. Besides, OAM waves with different OAM states generated by traveling-wave antennas with reflectors in [28] have much higher directivity and much closer divergence angels than OAM waves generated by transmitter without reflectors in [18]. Thus, different OAM waves can have approximate sizes of the circle regions due to their approximate divergence angles. In this case, circle regions of different OAM waves are assumed to have the same size in this paper. As shown in Fig. 1, the n^{th} $(1 \leq n \leq N)$ transmitting antenna is denoted as Tx_n and the m^{th} $(1 \leq m \leq M)$ receiving antenna is

denoted as Rx_m. The transmitting antenna array and receiving antenna array are assumed to be parallel with each other. Meanwhile, the receiving antenna Rx_m is configured at the circle region of the OAM wave transmitted by the corresponding transmitting antenna Tx_n when $m = n$. Thus the distance between Tx_n and Rx_m with $m = n$ is the same as the distance between Tx_j $(1 \le j \le N)$ and Rx_k $(1 \le k \le M)$ with $k = j$ considering the same radii of OAM waves' circle regions between all the transmitting and receiving antennas.

The cylindrical coordinate system (r, ϕ, z) is utilized to indicate locations of antennas in Fig. 1. The distance among adjacent transmitting or receiving antennas is configured as the same. Assuming Tx_n as the origin of the cylindrical coordinate system, the coordinate of Tx_j is expressed as $((j-n)\,\xi, 0, 0)$, where ξ is the distance between two adjacent transmitting antennas or receiving antennas. The location of Rx_m with $m = n$ is expressed by $\left(r_{\max}(z), \frac{\pi}{2}, z\right)$, where $r_{\max}(z)$ is the radius of the circle region at the position of z. Furthermore, the azimuth between Rx_m and Tx_n is written as

$$\phi_{mn} = \begin{cases} \arctan \dfrac{r_{\max}(z)}{|m-n|\,\xi}, & n < m \\ \pi - \arctan \dfrac{r_{\max}(z)}{|m-n|\,\xi}, & n > m \\ \pi/2, & n = m. \end{cases} \tag{1}$$

Therefore, the coordinate of Rx_m is expressed as (r_{mn}, ϕ_{mn}, z) with r_{mn} denoted by

$$r_{mn} = \sqrt{(|m-n|\,\xi)^2 + r_{\max}^2(z)}. \tag{2}$$

With the obtained coordinates, the transmission distance between Rx_m and Tx_n is derived as

$$d_{mn} = \sqrt{z^2 + (m-n)^2\xi^2 + r_{\max}^2(z)}. \tag{3}$$

B. OAM WIRELESS CHANNEL MODELS

In Fig. 1, the signal received by the receiving ULA is expressed as

$$\mathbf{Y} = \mathbf{H}\mathbf{X} + \mathbf{W}, \tag{4}$$

where $\mathbf{Y} = [y_1, \ldots, y_m, \ldots, y_M]^T \in \mathbb{C}^{M\times 1}$ is the received signal vector and y_m $(1 \le m \le M)$ is the signal received by the receiving antenna Rx_m. $\mathbf{X} = [x_1, \ldots, x_n, \ldots, x_N]^T \in \mathbb{C}^{N\times 1}$ is the transmitted signal vector and x_n $(1 \le n \le N)$ is the signal transmitted by the transmitting antenna Tx_n. $\mathbf{W} = [w_1, \ldots, w_m, \ldots, w_M]^T \in \mathbb{C}^{M\times 1}$ is the additive white Gaussian noise (AWGN) vector. The entries of $\mathbf{W}$ are assumed to be independent and identically distributed (*i.i.d*) complex Gaussian random variables with zero-mean and variance σ_n^2. The channel matrix $\mathbf{H} = \left[\mathbf{H}_1^l, \ldots, \mathbf{H}_n^l, \ldots, \mathbf{H}_N^l\right] \in \mathbb{C}^{M\times N}$ represents the channel response between the receiving antennas and transmitting antennas with the OAM state l, where $\mathbf{H}_n^l = \left[h_{1n}^l, \ldots, h_{mn}^l, \ldots, h_{Mn}^l\right]^T \in \mathbb{C}^{M\times 1}$ is the channel response between all the receiving antennas and the transmitting antenna Tx_n. h_{mn}^l is the channel response between Rx_m and Tx_n. Considering the location of the receiving antenna Rx_m, the channel response between Rx_m and Tx_n is modeled in following two cases:

Case 1: when $m = n$, the receiving antenna Rx_m is located within the circle region of the OAM wave generated by the transmitting antenna Tx_n. The channel response between Rx_n and Tx_n is expressed as

$$h_{nn}^l = \mathcal{B}\frac{\lambda}{4\pi d_{nn}} e^{-ikd_{nn}} e^{-i\frac{\pi}{2}l}, \tag{5}$$

where $\mathcal{B}$ is the channel gain coefficient which represents the variation of attenuation and phase during the wireless propagation, λ is the wavelength, $k = 2\pi/\lambda$ is the wave number, d_{nn} is the distance between Rx_n and Tx_n and calculated based on (3), $e^{-i\frac{\pi}{2}l}$ is the OAM wave helical phase term with l being the OAM state [30]. Based on (5), the OAM signal propagates within a circle region. Moreover, the OAM signal propagation within the circle region follows the Friis Formula and the OAM signal attenuates with the inverse square of the transmission distance [24]. Hence, $\mathcal{B}$ is configured as a constant in this paper.

Case 2: when $m \ne n$, the receiving antenna Rx_m is located outside the circle region of the OAM wave generated by the transmitting antenna Tx_n. The channel response between Rx_m and Tx_n is expressed as

$$h_{mn}^l = \mathcal{B}_{mn}\frac{\lambda}{4\pi d_{mn}} e^{-ikd_{mn}} e^{-il\phi_{mn}}, \tag{6}$$

where $\mathcal{B}_{mn}$ is the channel gain coefficient between Rx_m and Tx_n. Because the receiving antenna Rx_m locates outside the circle region of the OAM wave transmitted by Tx_n, the attenuation of the OAM signal between Rx_m and Tx_n does not follow the inverse square of the transmission distance. Therefore, the channel gain coefficient $\mathcal{B}_{mn}$ should be modeled by the spatial energy distribution characteristics of OAM waves.

The intensity of the OAM wave generated by the traveling-wave antenna is focused within the circle region [27]. Along with the helical phase front, the OAM wave is described by the Laguerre-Gaussian beams [11], [24]. In cylindrical coordinate system, the Laguerre-Gaussian beams are expressed by

$$u(r,\phi,z) = \alpha\sqrt{\frac{p!}{\pi\,(p+|l|)!}}\frac{1}{w(z)}\left(\frac{r\sqrt{2}}{w(z)}\right)^{|l|} e^{-\left(\frac{r}{w(z)}\right)^2} \times L_p^{|l|}\left(\frac{2r^2}{w^2(z)}\right) e^{-i\frac{\pi r^2}{\lambda R(z)}} e^{i(|l|+2p+1)\psi(z)} e^{-il\phi}, \tag{7a}$$

with

$$R(z) = z\left[1 + \left(\frac{\pi w_l^2}{\lambda z}\right)^2\right], \tag{7b}$$

$$w(z) = w_l\sqrt{1 + \left(\frac{z}{z_R}\right)^2}, \tag{7c}$$

where the term $\alpha\sqrt{\frac{p!}{\pi(p+|l|)!}}$ is a normalized constant, p is the radial index which represents the number of radial nodes

in the intensity distribution. In generally, p is configured as 0 for OAM-based MIMO communication systems [19]. $w(z)$ is the radius where the amplitude falls into the $\frac{1}{e}$ of the axial value at the position of z. $z_R = \frac{\pi w_l^2}{\lambda}$ is the Rayleigh distance and w_l is the beam waist radius with the OAM state l at $z = 0$. $L_p^{|l|}\left(\frac{2r^2}{w^2(z)}\right)$ is the generalized Laguerre polynomial. $e^{-jl\phi}$ represents the helical phase distribution. $\psi(z) = arctan\left(\frac{z}{z_R}\right)$ is the Gouy phase. The energy of the OAM wave is focused in the circle region, which is characterized by the Laguerre-Gaussian beam in (7). The radius of the OAM circle region with the maximum energy strength is denoted by

$$r_{\max}(z) = \sqrt{\frac{|l|}{2}} w(z) = w_l \sqrt{\frac{|l|}{2}\left(1 + \left(\frac{z}{z_R}\right)^2\right)}. \tag{8}$$

As described in the system model, the radii of the OAM waves' circle regions corresponding to different transmitting antennas are configured the same [23]. Assuming that the beam waist w_{l_1} with the OAM state l_1 is constant, for other OAM waves with OAM state l_n ($n \neq 1$), the following equation should be satisfied:

$$w_{l_1} \sqrt{\frac{|l_1|}{2}\left(1 + \left(\frac{z}{z_R}\right)^2\right)} = w_{l_n} \sqrt{\frac{|l_n|}{2}\left(1 + \left(\frac{z}{z_R}\right)^2\right)}. \tag{9}$$

Substituting the Rayleigh distance $z_R = \frac{\pi w_l^2}{\lambda}$ into (9), (9) is transformed into

$$A w_{l_n}^4 - B w_{l_n}^2 + C = 0, \tag{10a}$$

with

$$A = w_{l_1}^2 |l_n| \pi^2, \tag{10b}$$
$$B = |l_1| (\pi^2 w_{l_1}^4 + z^2 \lambda^2), \tag{10c}$$
$$C = w_{l_1}^2 |l_n| z^2 \lambda^2. \tag{10d}$$

The beam waist w_{l_n} with OAM state l_n can be solved by (10). Substituting w_{l_n} into (7), the strength distribution of OAM waves with OAM state l_n is obtained. Meanwhile, $u(r, \phi, z)$ in (7) can be regarded as the response of the OAM electromagnetic wave in the cylindrical coordinate system with the input of a unit pulse. When the OAM wave with OAM state l is transmitted by the transmitting antenna Tx_n, the response u_{nn} at the receiving antenna Rx_m with $m = n$ is expressed as $u_{nn} = h_{nn}^l \hat{x}$, where $\hat{x}$ denotes the unit pulse input. The response u_{mn} at the receiving antenna Rx_m with $m \neq n$ is expressed as $u_{mn} = h_{mn}^l \hat{x}$. Thus, the following proportion relationship is derived as

$$\frac{u_{mn}}{u_{nn}} = \frac{h_{mn}^l}{h_{nn}^l}. \tag{11}$$

Based on channel response functions in (5) and (6), the right side of (11) is written as

$$\begin{aligned} \frac{h_{mn}^l}{h_{nn}^l} &= \frac{\mathcal{B}_{mn} \frac{\lambda}{4\pi d_{mn}} e^{-ikd_{mn}} e^{-il_n\phi_{mn}}}{\mathcal{B} \frac{\lambda}{4\pi d_{nn}} e^{-ikd_{nn}} e^{-il_n\phi_{nn}}} \\ &= \frac{\mathcal{B}_{mn} d_{nn}}{\mathcal{B} d_{mn}} e^{-ik(d_{mn}-d_{nn})} e^{-il_n(\phi_{mn}-\phi_{nn})}. \end{aligned} \tag{12}$$

Based on the Laguerre-Gaussian beam in (7), the left side of (11) is transformed into

$$\begin{aligned} \frac{u_{mn}}{u_{nn}} &= \frac{\alpha \sqrt{\frac{1}{\pi |l_n|!}} \frac{1}{w_n(z)} \left(\frac{r_{mn}\sqrt{2}}{w_n(z)}\right)^{|l_n|} e^{-\left(\frac{r_{mn}}{w_n(z)}\right)^2}}{\alpha \sqrt{\frac{1}{\pi |l_n|!}} \frac{1}{w_n(z)} \left(\frac{r_{nn}\sqrt{2}}{w_n(z)}\right)^{|l_n|} e^{-\left(\frac{r_{nn}}{w_n(z)}\right)^2}} \\ &\quad \times \frac{e^{-i\frac{\pi r_{mn}^2}{\lambda R_n(z)}} e^{i(|l_n|+1)\psi_n(z)} e^{-il_n\phi_{mn}}}{e^{-i\frac{\pi r_{nn}^2}{\lambda R_n(z)}} e^{i(|l_n|+1)\psi_n(z)} e^{-il_n\phi_{nn}}} \\ &= \frac{(r_{mn})^{|l_n|} e^{-\left(\frac{r_{mn}}{w_n(z)}\right)^2} e^{-i\frac{\pi r_{mn}^2}{\lambda R_n(z)}} e^{-il_n\phi_{mn}}}{(r_{nn})^{|l_n|} e^{-\left(\frac{r_{nn}}{w_n(z)}\right)^2} e^{-i\frac{\pi r_{nn}^2}{\lambda R_n(z)}} e^{-il_n\phi_{nn}}} \\ &= \left(\frac{r_{mn}}{r_{nn}}\right)^{|l_n|} e^{-\frac{r_{mn}^2 - r_{nn}^2}{w_n^2(z)}} e^{-i\frac{\pi(r_{mn}^2 - r_{nn}^2)}{\lambda R_n(z)}} \\ &\quad \times e^{-il_n(\phi_{mn}-\phi_{nn})}. \end{aligned} \tag{13}$$

Based on (12) and (13), the channel gain coefficient $\mathcal{B}_{mn}$ is derived as

$$\begin{aligned} \mathcal{B}_{mn} &= \frac{u_{mn}}{u_{nn}} h_{nn}^l \frac{4\pi d_{mn}}{\lambda} e^{ikd_{mn}} e^{il\phi_{mn}} \\ &= \mathcal{B} \frac{d_{mn}}{d_{nn}} \left(\frac{r_{mn}}{r_{nn}}\right)^{|l_n|} e^{-\frac{r_{mn}^2 - r_{nn}^2}{w_n^2(z)}} e^{-i\frac{\pi(r_{mn}^2 - r_{nn}^2)}{\lambda R_n(z)}} \\ &\quad \times e^{ik(d_{mn}-d_{nn})}. \end{aligned} \tag{14}$$

Substituting (14) into (6), the channel response between Rx_m and Tx_n is expressed as

$$\begin{aligned} h_{mn}^l = \mathcal{B} \frac{\lambda}{4\pi d_{nn}} \left(\frac{r_{mn}}{r_{nn}}\right)^{|l_n|} e^{-\frac{r_{mn}^2 - r_{nn}^2}{w_n^2(z)}} e^{-i\frac{\pi(r_{mn}^2 - r_{nn}^2)}{\lambda R_n(z)}} \\ \times e^{-ikd_{nn}} e^{-il_n\phi_{mn}}. \end{aligned} \tag{15}$$

Considering the spatial distribution characteristics of OAM waves, the OAM wireless channel model is modeled as (5) and (15) for OAM-based MIMO communication systems.

C. CAPACITY OF OAM-BASED MIMO COMMUNICATION SYSTEMS

To derive the capacity of the OAM-based MIMO communication system, as the first step, the singular value decomposition (SVD) of the OAM channel matrix is expressed by

$$\mathbf{H}_{\mathrm{MN}}^{\mathrm{OAM}} = \mathbf{U} \Sigma \mathbf{V}^H, \tag{16}$$

where $\mathbf{U} \in \mathbb{C}^{M \times M}$ and $\mathbf{V} \in \mathbb{C}^{N \times N}$ are unitary matrixes and $\mathbf{U}$ contains the left singular vectors of $\mathbf{H}_{\mathrm{MN}}^{\mathrm{OAM}}$, $\mathbf{V}$ contains the right singular vectors of $\mathbf{H}_{\mathrm{MN}}^{\mathrm{OAM}}$, H is the conjugate transition operation. $\mathbf{\Sigma} \in \mathbb{C}^{M \times N}$ is a diagonal matrix with positive

singular values $\delta_1^{oam}, \delta_2^{oam}, \delta_3^{oam} \cdots \delta_\gamma^{oam}$ in decreasing order, where γ is the rank of $\mathbf{H}_{\mathrm{MN}}^{\mathrm{OAM}}$.

For an OAM-based MIMO communication system, the transmitted signal vector $\mathbf{X}$ can be expressed as the product from of the unitary matrix $\mathbf{V}$ and a new vector $\widetilde{\mathbf{X}}$. Similarly, we obtained another new vector $\widetilde{\mathbf{Y}}$ by multiplying received vector $\mathbf{Y}$ with the unitary matrix $\mathbf{U}^H$. $\mathbf{X}$ and $\widetilde{\mathbf{Y}}$ are expressed as

$$\mathbf{X} = \mathbf{V}\widetilde{\mathbf{X}}, \tag{17}$$

$$\widetilde{\mathbf{Y}} = \mathbf{U}^H\mathbf{Y}. \tag{18}$$

Furthermore, we perform these operations on the OAM-based MIMO communication system and these operations change nothing from a capacity point of view [31]. For the OAM-based MIMO communication system, an equivalent system is obtained and denoted by

$$\begin{aligned}\widetilde{\mathbf{Y}} &= \mathbf{U}^H\mathbf{Y} \\ &= \mathbf{U}^H\left(\mathbf{H}_{\mathrm{MN}}^{\mathrm{OAM}}\mathbf{V}\widetilde{\mathbf{X}} + \mathbf{W}\right) \\ &= \mathbf{U}^H\mathbf{H}_{\mathrm{MN}}^{\mathrm{OAM}}\mathbf{V}\widetilde{\mathbf{X}} + \mathbf{U}^H\mathbf{W} \\ &= \mathbf{\Sigma}\widetilde{\mathbf{X}} + \widetilde{\mathbf{W}}. \end{aligned} \tag{19}$$

When the new channel noise is calculated by $\widetilde{\mathbf{W}} = \mathbf{U}^H\mathbf{W}$, the new channel noise vector has the same distribution as $\mathbf{W}$ since $\mathbf{U}$ is unitary matrix. Based on the SVD of OAM channel matrix, the capacity C^{OAM} of OAM-based MIMO communication system at the transmitter is expressed as

$$C^{\mathrm{OAM}}(P) = \sum_{i=1}^{\gamma} \log_2\left(1 + \frac{P_i}{\sigma_n^2/\left(\delta_i^{mimo}\right)^2}\right), \tag{20}$$

where σ_n^2 is the receiver noise variance and the sum of all the available power P is assumed to be distributed across the channels based on the water-filling principle, such that

$$P = \sum_{i=1}^{\gamma} P_i. \tag{21}$$

Besides, the condition number of OAM channel matrix $\mathbf{H}_{\mathrm{MN}}^{\mathrm{OAM}}$ is defined as

$$k^{\mathrm{OAM}} = cond\left(\mathbf{H}_{\mathrm{MN}}^{\mathrm{OAM}}\right) = \frac{\max\left(\delta_i^{oam}\right)}{\min\left(\delta_i^{oam}\right)}. \tag{22}$$

In generally, the wireless channel is the better when the value of k^{OAM} is nearer to 1 [22], [32].

For the conventional MIMO communication systems, the channel response between Rx_m and Tx_n is expressed as

$$h_{mn}^{\mathrm{MIMO}} = \mathcal{B}\frac{\lambda}{4\pi d_{mn}}e^{-ikd_{mn}}. \tag{23}$$

Without loss of generality, in this paper the transmitting antennas are configured as omnidirectional antennas for conventional MIMO communication systems. The channel gain coefficient is configured as a constant in conventional MIMO communication systems. It is easy to be found that OAM-based MIMO communication system and conventional MIMO communication system only differ in the type of transmitting antennas in this paper. The OAM wave is transmitted by traveling-wave antennas in OAM-based MIMO communication systems. The plane wave is transmitted by ordinary antennas in conventional MIMO communication systems. Hence, the process of calculating the capacity of MIMO communication systems is the same with that of OAM-based MIMO communication systems. Therefore, the capacity of MIMO communication system is obtained by replacing the OAM-based MIMO channel matrix $\mathbf{H}_{\mathrm{MN}}^{\mathrm{OAM}}$ with the MIMO channel matrix $\mathbf{H}_{\mathrm{MN}}^{\mathrm{MIMO}}$ when the SVD method is adopted. The corresponding capacity C^{MIMO} of MIMO communication systems at the transmitter is expressed as

$$C^{\mathrm{MIMO}}(P) = \sum_{i=1}^{\gamma} \log_2\left(1 + \frac{P_i}{\sigma_n^2/\left(\delta_i^{oam}\right)^2}\right), \tag{24}$$

where δ_i^{mimo} denotes the i^{th} positive singular values of $\delta_1^{mimo}, \delta_2^{mimo}, \delta_3^{mimo} \cdot \cdot, \delta_\gamma^{mimo}$ in decreasing order, γ is the rank of $\mathbf{H}_{\mathrm{MN}}^{\mathrm{MIMO}}$.

For MIMO communication systems, the condition number [22], [32] of channel matrix $\mathbf{H}_{\mathrm{MN}}^{\mathrm{MIMO}}$ is expressed as

$$k^{\mathrm{MIMO}} = cond\left(\mathbf{H}_{\mathrm{MN}}^{\mathrm{MIMO}}\right) = \frac{\max\left(\delta_i^{mimo}\right)}{\min\left(\delta_i^{mimo}\right)}. \tag{25}$$

III. SIMULATION RESULTS AND DISCUSSIONS

In this section, the propagation gains inside and outside the circle region of OAM waves are considered and compared for both the proposed OAM wireless channel model and the conventional OAM wireless channel model. Besides, based on the proposed capacity model of OAM-based MIMO communication system, the system performance of OAM-based MIMO, conventional OAM and conventional MIMO communication systems is compared and analyzed. To simplify simulations, the number of transmitting antennas is configured to be equal to the number of receiving antennas. The default simulation parameters are configured as follows: the carrier frequency is 70 GHz and λ is the corresponding carrier wavelength. The transmission signal-to-noise ratio (SNR) is configured as 20 dB. The distance between adjacent antennas, *i.e.*, the antenna spacing ξ is configured as 10λ. The beam waist of the first transmitting antenna is 2λ. The OAM states of transmitted OAM waves are evenly distributed with an OAM state interval ΔL configured as 20. When the antenna array is configured as 4×4, the OAM states of OAM waves radiated from transmitting antennas are $l_1 = -30,\ l_2 = -10, l_3 = 10,\ l_4 = 30$.

Fig. 2 illustrates the propagation gains inside and outside the circle region for both the proposed OAM and conventional OAM wireless channel models. In Fig. 2(a), $|h_{11}|^2$ is used as the propagation gain inside the circle region. In Fig. 2(b), $|h_{m5}|^2$ is used as the propagation gain. In this case, m denotes the m^{th} receiving antenna and $|h_{m5}|^2$ denotes the propagation gain between the 5^{th} transmitting antenna and all the receiving antennas. Therefore, $|h_{55}|^2$ is the propagation gain inside

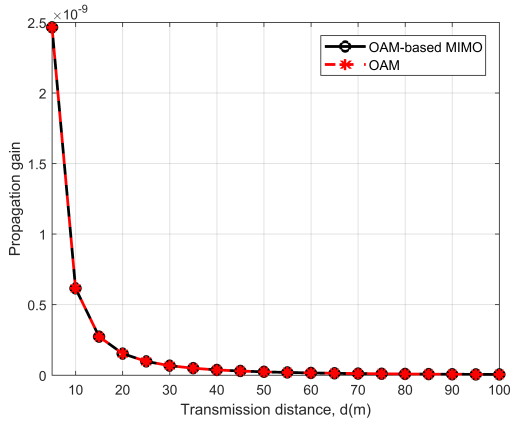

(a)

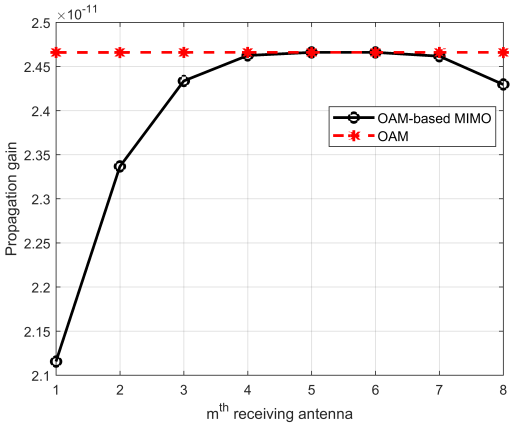

(b)

FIGURE 2. Propagation gains inside and outside the circle region for the OAM-based MIMO and the conventional OAM wireless channel models. (a) Propagation gain inside the circle region; (b) Propagation gain outside the circle region.

the circle region and $|h_{m5}|^2$ is the propagation gain outside the circle region when $m \neq 5$. When m is closer to 5, the m^{th} receiving antenna is closer to the circle region of OAM wave generated by the 5^{th} transmitting antenna. From Fig. 2(a), it can be seen that the propagation gains inside the circle region remain the same for the proposed and conventional OAM channel models with the increase of the transmission distance. From Fig. 2(b), it can be seen that the propagation gains outside the circle region are different for the proposed and conventional OAM channel models. Besides, the curve in Fig. 2(b) is a concave curve and the propagation gain is maximized at $m = 5$, namely, the propagation gain increases when m is closer to 5. Thus, because the m^{th} receiving antenna is closer to the circle region of OAM wave generated by the 5^{th} transmitting antenna when m is closer to 5, Fig. 2(b) illustrates that the propagation gain increases with the decrease of the distance from the circle region.

Fig. 3 illustrates the capacity with respect to the transmission distance considering OAM-based MIMO, conventional OAM and conventional MIMO communication systems. When the antenna array is fixed, the capacity of

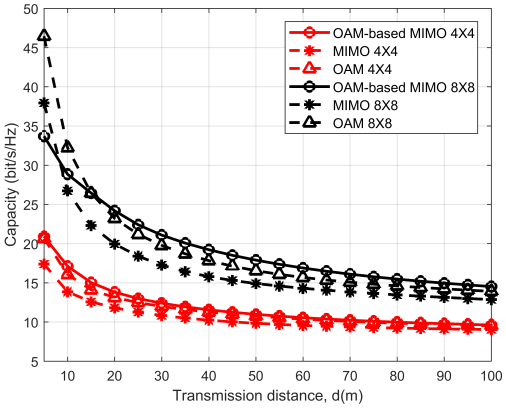

FIGURE 3. Capacity with respect to the transmission distance considering different antenna array configurations.

OAM-based MIMO, conventional OAM and conventional MIMO communication systems always decrease with the increase of the transmission distance. Moreover, the capacity of OAM-based MIMO, conventional OAM and conventional MIMO communication systems with 8×8 antenna array is larger than the capacity of OAM-based MIMO, conventional OAM and conventional MIMO communication systems with 4×4 antenna array. When the antenna array is configured as 4×4 and the transmission distance is fixed, the capacity of OAM-based MIMO communication systems is larger than the capacity of both conventional OAM and conventional MIMO communication systems. When the antenna array is configured as 8×8 and the transmission distance is less than 15 meters, the capacity of OAM-based MIMO communication systems is less than the capacity of conventional OAM communication systems. When the antenna array is configured as 8×8 and the transmission distance is larger than or equal to 15 meters, the capacity of OAM-based MIMO communication systems is larger than or equal to the capacity of conventional OAM communication systems. When the antenna array is configured as 8×8 and the transmission distance is less than 8 meters, the capacity of OAM-based MIMO communication systems is less than the capacity of conventional MIMO communication systems. When the antenna array is configured as 8×8 and the transmission distance is larger than or equal to 8 meters, the capacity of OAM-based MIMO communication systems is larger than or equal to the capacity of conventional MIMO communication systems.

Fig. 4 shows the capacity of OAM-based MIMO communication systems with respect to the transmission distance considering different OAM state intervals. Without loss of generality, the antenna array is configured as 4×4. When the transmission distance is fixed, the capacity of OAM-based MIMO communication systems increase with the increase of OAM state intervals. Moreover, the impact of OAM state intervals on the capacity becomes weaker as the transmission distance increases.

When the transmission distance is configured as 50 meters, Fig. 5 describes the capacity of OAM-based MIMO,

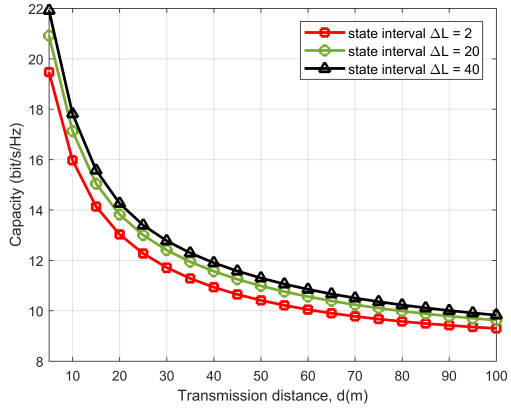

FIGURE 4. Capacity of OAM-based MIMO communication systems with respect to the transmission distance considering different OAM state intervals.

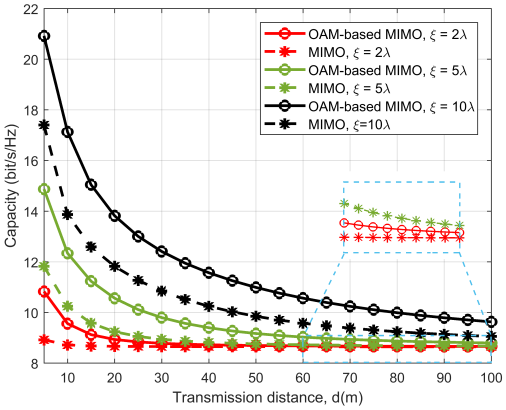

FIGURE 6. Capacity with respect to the transmission distance considering different antenna spacings.

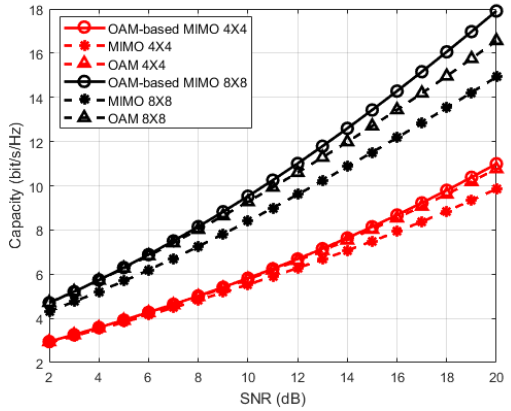

FIGURE 5. Capacity with respect to the transmission SNR considering different antenna array configurations.

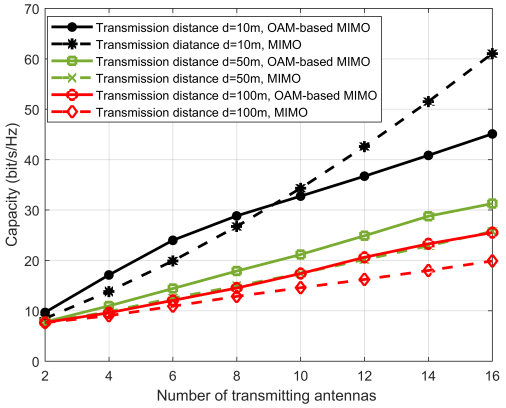

FIGURE 7. Capacity with respect to the number of transmitting antennas considering different transmission distances.

conventional OAM and conventional MIMO communication systems with respect to the transmission SNR considering different antenna array configurations. When the antenna array is fixed, the capacity increases with the increase of transmission SNR. When the transmission SNR is fixed, the capacity of OAM-based MIMO communication systems is larger than the capacity of conventional OAM and conventional MIMO communication systems. When the transmission SNR is fixed, the capacity of OAM-based MIMO, conventional OAM and conventional MIMO communication systems with 8×8 antenna array is larger than the capacity of OAM-based MIMO, conventional OAM and conventional MIMO communication systems with 4×4 antenna array.

Fig. 6 illustrates the capacity of OAM-based MIMO and conventional MIMO communication systems with respect to the transmission distance considering different antenna spacings ξ. Without loss of generality, the antenna array is configured as 4×4. When the transmission distance is fixed, the capacity of both OAM-based MIMO and conventional MIMO communication systems increases with the increase of the antenna spacing. When the antenna spacing is fixed, the capacity of OAM-based MIMO communication systems is larger than the capacity of conventional MIMO communication systems.

Fig. 7 illustrates the capacity of OAM-based MIMO and conventional MIMO communication systems with respect to the number of transmitting antennas considering different transmission distances. The number of receiving antennas is configured to be equal to the number of transmitting antennas in numerical simulations. When the transmission distance is fixed, the capacity of OAM-based MIMO and conventional MIMO communication systems increases with the increase of the number of transmitting antennas. When the number of transmitting antennas is fixed, the capacity of OAM-based MIMO and conventional MIMO communication systems decreases with the increase of the transmission distances. Besides, the capacity of OAM-based MIMO system is larger than the capacity of conventional MIMO system when the transmission distance is larger than a specific threshold. These thresholds in Fig. 7 increase with the increase of the number of transmitting antennas in OAM-based MIMO and conventional MIMO communication systems.

In Fig. 8, the average condition numbers of wireless channels with respect to the transmission distance is compared for

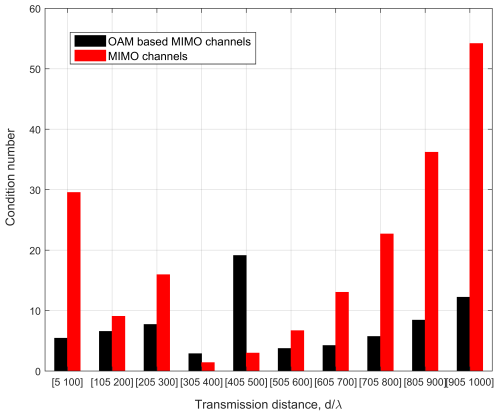

FIGURE 8. Average condition number of wireless channels with respect to the transmission distance.

OAM-based MIMO and conventional MIMO communication systems. The antenna array is configured as 4×4 and the transmission distance is an integral multiple of λ. When the transmission distance is less than 300λ or larger than 505λ, the average condition number of wireless channels in OAM-based MIMO communication systems is less than the average condition number of wireless channels in conventional MIMO communication systems. Based on the result in [32], wireless channels are more conducive to wireless transmissions when the condition number of wireless channel is close to 1, *i.e.*, the wireless channel is well-conditioned. Moreover, the channel becomes more sensitive to changes, such as noise, when the condition number is bigger than 1 [22]. Thus, when the transmission distance is less than 300λ or larger than 505λ, OAM wireless channels are more conducive to wireless transmissions than conventional MIMO channels. When the transmission distance is between 305λ and 500λ, the average condition number of wireless channels in OAM-based MIMO communication systems is larger than the average condition number of wireless channels in conventional MIMO communication systems. In this case, conventional MIMO channels are more conducive to wireless transmissions than OAM wireless channels.

IV. CONCLUSIONS

In this paper, an OAM wireless channel model has been proposed based on the spatial energy distribution characteristics of OAM waves. Moreover, the capacity of OAM-based MIMO communication system has been derived based on the proposed OAM wireless channel model. Simulation results have shown that the channel capacity of OAM-based MIMO communication system is larger than the channel capacity of conventional OAM and conventional MIMO communication systems when the transmission distance is larger than a specific threshold. In addition, the effects of some system parameters, such as OAM state interval and antenna spacing, on the capacity of OAM-based MIMO communication system have been investigated. Simulation results have shown that larger OAM state intervals and larger antenna spacings can increase the channel capacity for OAM-based MIMO communication systems. Our results provide some guidelines to evaluate the capacity of OAM-based MIMO communication systems.

REFERENCES

[1] J. Thompson *et al.*, "5G wireless communication systems: Prospects and challenges [guest editorial]," *IEEE Commun. Mag.*, vol. 52, no. 2, pp. 62–64, Feb. 2014.
[2] C.-X. Wang *et al.*, "Cellular architecture and key technologies for 5G wireless communication networks," *IEEE Commun. Mag.*, vol. 52, no. 2, pp. 122–130, Feb. 2014.
[3] G. Mao and B. D. Anderson, "Capacity of large wireless networks with generally distributed nodes," *IEEE Trans. Wireless Commun.*, vol. 13, no. 3, pp. 1678–1691, Mar. 2014.
[4] X. Ge, S. Tu, G. Mao, and C. X. Wang, "5G ultra-dense cellular networks," *IEEE Trans. Wireless Commun.*, vol. 23, no. 1, pp. 72–79, Feb. 2016.
[5] X. Ge, B. Yang, J. Ye, G. Mao, C.-X. Wang, and T. Han, "Spatial spectrum and energy efficiency of random cellular networks," *IEEE Trans. Commun.*, vol. 63, no. 3, pp. 1019–1030, Mar. 2015.
[6] R. Zi, X. Ge, J. Thompson, C.-X. Wang, H. Wang, and T. Han, "Energy efficiency optimization of 5G radio frequency chain systems," *IEEE J. Sel. Areas Commun.*, vol. 34, no. 4, pp. 758–771, Apr. 2016.
[7] A. Goldsmith, *Wireless Communications*. Cambridge, U.K.: Cambridge Univ. Press, 2005.
[8] R. A. Beth, "Mechanical detection and measurement of the angular momentum of light," *Phys. Rev.*, vol. 50, pp. 115–127, Jul. 1936.
[9] J. D. Jackson and R. F. Fox, "Classical electrodynamics," *Amer. J. Phys.*, vol. 67, no. 9, pp. 841–842, 1999.
[10] L. Allen, M. W. Beijersbergen, R. J. C. Spreeuw, and J. P. Woerdman, "Orbital angular momentum of light and the transformation of Laguerre–Gaussian laser modes," *Phys. Rev. A, Gen. Phys.*, vol. 45, no. 11, pp. 8185–8190, Jun. 1992.
[11] A. M. Yao and M. J. Padgett, "Orbital angular momentum: Origins, behavior and applications," *Adv. Opt. Photon.*, vol. 3, no. 3, pp. 161–204, May 2011.
[12] M. P. J. Lavery, F. C. Speirits, S. M. Barnett, and M. J. Padgett, "Detection of a spinning object using light's orbital angular momentum," *Science*, vol. 341, no. 6145, pp. 537–540, 2013.
[13] G. Gibson, J. Courtial, M. J. Padgett, M. Vasnetsov, and V. Pas'ko, "Free-space information transfer using light beams carrying orbital angular momentum," *Opt. Exp.*, vol. 12, no. 22, pp. 5448–5456, Nov. 2004.
[14] A. E. Willner *et al.*, "Optical communications using orbital angular momentum beams," *Adv. Opt. Photon.*, vol. 7, no. 1, pp. 66–106, Mar. 2015.
[15] S. H. Murshid and A. Khayrattee, "Multiplexing of optical channels as a function of orbital angular momentum of photons," in *Proc. FiO/LS XXIV Conf., OSA Tech. Dig. (CD) (Opt. Soc. Amer.)*, Rochester, NY, USA, Oct. 2008, p. 1.
[16] J. Wang *et al.*, "Terabit free-space data transmission employing orbital angular momentum multiplexing," *Nature Photon.*, vol. 6, pp. 488–496, Jun. 2012.
[17] S. Li and J. Wang, "A compact trench-assisted multi-orbital-angular-momentum multi-ring fiber for ultrahigh-density space-division multiplexing (19 rings × 22 modes)," *Sci. Rep.*, vol. 4, Jan. 2014, Art. no. 3853.
[18] S. M. Mohammadi *et al.*, "Orbital angular momentum in radio—A system study," *IEEE Trans. Antennas Propag.*, vol. 58, no. 2, pp. 565–572, Feb. 2010.
[19] F. Tamburini, E. Mari, A. Sponselli, B. Thidé, A. Bianchini, and F. Romanato, "Encoding many channels on the same frequency through radio vorticity: First experimental test," *New J. Phys.*, vol. 14, no. 3, p. 033001, Mar. 2012.
[20] O. Edfors and A. J. Johansson, "Is orbital angular momentum (OAM) based radio communication an unexploited area?" *IEEE Trans. Antennas Propag.*, vol. 60, no. 2, pp. 1126–1131, Feb. 2012.
[21] A. Cagliero and R. Gaffoglio, "On the spectral efficiency limits of an OAM-based multiplexing scheme," *IEEE Antennas Wireless Propag. Lett.*, vol. 16, pp. 900–903, Oct. 2016.
[22] K. A. Opare and Y. Kuang, "Performance of an ideal wireless orbital angular momentum communication system using multiple-input multiple-output techniques," in *Proc. Int. Conf. TEMU*, Heraklion, Greece, Jul. 2014, pp. 144–149.
[23] A. Zhang, S. Zheng, Y. Chen, X. Jin, H. Chi, and X. Zhang, "The capacity gain of orbital angular momentum based multiple-input-multiple-output system," *Sci. Rep.*, vol. 6, May 2016, Art. no. 25418.

[24] M. Oldoni *et al.*, "Space-division demultiplexing in orbital-angular-momentum-based MIMO radio systems," *IEEE Trans. Antennas Propag.*, vol. 63, no. 10, pp. 4582–4587, Oct. 2015.
[25] M. J. Padgett, F. M. Miatto, M. P. J. Lavery, A. Zeilinger, and R. W. Boyd, "Divergence of an orbital-angular-momentum-carrying beam upon propagation," *New J. Phys.*, vol. 17, no. 2, p. 023011, Feb. 2015.
[26] W. Zhang *et al.*, "Mode division multiplexing communication using microwave orbital angular momentum: An experimental study," *IEEE Trans. Wireless Commun.*, vol. 16, no. 2, pp. 1308–1318, Feb. 2017.
[27] X. Hui *et al.*, "Multiplexed millimeter wave communication with dual orbital angular momentum (OAM) mode antennas," *Sci. Rep.*, vol. 5, May 2015, Art. no. 10148.
[28] W. Zhang *et al.*, "Four-OAM-mode antenna with traveling-wave ring-slot structure," *IEEE Antennas Wireless Propag. Lett.*, vol. 16, pp. 194–197, May 2016.
[29] S. Zheng, X. Hui, X. Jin, H. Chi, and X. Zhang, "Transmission characteristics of a twisted radio wave based on circular traveling-wave antenna," *IEEE Trans. Antennas Propag.*, vol. 63, no. 4, pp. 1530–1536, Apr. 2015.
[30] Y. Yan *et al.*, "High-capacity millimetre-wave communications with orbital angular momentum multiplexing," *Nature Commun.*, vol. 5, Sep. 2014, Art. no. 4876.
[31] İ. E. Telatar, "Capacity of multi-antenna Gaussian channels," *Eur. Trans. Telecommun.*, vol. 10, no. 6, pp. 585–595, Sep. 1999.
[32] Y. Yuan, Z. Zhang, J. Cang, H. Wu, and C. Zhong, "Capacity analysis of UCA-based OAM multiplexing communication system," in *Proc. Int. Conf. WCSP*, London, U.K., Oct. 2015, pp. 1–5.

LIANG WANG received the B.E. degree in communication engineering from the Huazhong University of Science and Technology, Wuhan, China, in 2016, where she is currently pursuing the M.S. degree. Her research interests mainly in the orbital angular momentum technology.

XIAOHU GE (M'09–SM'11) received the Ph.D. degree in communication and information engineering from the Huazhong University of Science and Technology (HUST), Wuhan, China, in 2003. He is currently a Full Professor with the School of Electronic Information and Communications, HUST. He is also an Adjunct Professor with the Faculty of Engineering and Information Technology, The University of Technology Sydney, Sydney, NSW, Australia. He has been with HUST since 2005. Prior to that, he was a Researcher with Ajou University, Suwon, South Korea, and Politecnico Di Torino, Turin, Italy, from 2004 to 2005. He was a Visiting Researcher with Heriot-Watt University, Edinburgh, U.K., from to 2010. He has authored about 100 papers in refereed journals and conference proceedings and has been granted about 15 patents in China. His research interests include mobile communications, traffic modeling in wireless networks, green communications, and interference modeling in wireless communications. He is leading several projects funded by NSFC, China, MOST, and industries. He is taking part in several international joint projects, such as the EU FP7-PEOPLE-IRSES: the project WiNDOW and the project CROWN.

Dr. Ge is a Senior Member of the China Institute of Communications and a member of the National Natural Science Foundation of China and the Chinese Ministry of Science and Technology Peer Review College. He has been actively involved in organizing more than ten international conferences since 2005. He served as the General Chair for the 2015 IEEE International Conference on Green Computing and Communications (IEEE GreenCom). He serves as an Associate Editor for the IEEE ACCESS, *Wireless Communications and Mobile Computing Journal* (Wiley), and the *International Journal of Communication Systems* (Wiley). Moreover, he served as a Guest Editor for the *IEEE Communications Magazine Special Issue on 5G Wireless Communication Systems*. He was a recipient of Best Paper Awards from the IEEE Globecom 2010.

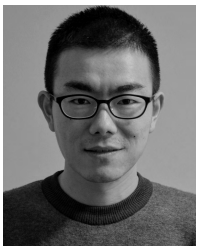

RAN ZI (S'14) received the B.E., M.S. and Ph.D. degrees in information and communication engineering from the Huazhong University of Science and Technology, Wuhan, China, in 2011, 2013, and 2017, respectively. He was a Visiting Scholar with the University of Sheffield, Sheffield, U.K., during 2015 and 2016. He is currently with Sangfor Technology Co., Shenzhen, China. His research interests include MIMO systems, millimeter wave communications, orbital angular momentum transmissions, and physical-layer security. He received the National Scholarship for Ph.D. students in 2016.

CHENG-XIANG WANG (S'01–M'05–SM'08–F'17) received the B.Sc. and M.Eng. degrees in communication and information systems from Shandong University, China, in 1997 and 2000, respectively, and the Ph.D. degree in wireless communications from Aalborg University, Denmark, in 2004.

He was a Research Fellow with the University of Agder, Grimstad, Norway, from 2001 to 2005, a Visiting Researcher with Siemens AG Mobile Phones, Munich, Germany, in 2004, and a Research Assistant with the Hamburg University of Technology, Hamburg, Germany, from 2000 to 2001. He has been with Heriot-Watt University, Edinburgh, U.K., since 2005, where he was promoted to a Professor in 2011. He is also an Honorary Fellow of the University of Edinburgh, U.K., and a Chair/Guest Professor of Shandong University and Southeast University, China. He has authored one book, one book chapter, and over 300 papers in refereed journals and conference proceedings. His current research interests include wireless channel modeling and (B)5G wireless communication networks, including green communications, cognitive radio networks, high mobility communication networks, massive MIMO, millimeter wave communications, and visible light communications.

Dr. Wang is a fellow of the IET and HEA, and a member of the EPSRC Peer Review College. He served or is currently serving as an Editor for nine international journals, including the IEEE TRANSACTIONS ON VEHICULAR TECHNOLOGY since 2011, the IEEE TRANSACTIONS ON COMMUNICATIONS since 2015, and the IEEE TRANSACTIONS ON WIRELESS COMMUNICATIONS from 2007 to 2009. He was the Leading Guest Editor of the IEEE JOURNAL ON SELECTED AREAS IN COMMUNICATIONS—Special Issue on Vehicular Communications and Networks. He is also a Guest Editor of the IEEE JOURNAL ON SELECTED AREAS IN COMMUNICATIONS—Special Issue on Spectrum and Energy Efficient Design of Wireless Communication Networks, and the IEEE TRANSACTIONS ON BIG DATA—Special Issue on Wireless Big Data. He served or is serving as a TPC Member, the TPC Chair, and the General Chair of over 80 international conferences. He received nine best paper awards from the IEEE Globecom 2010, the IEEE ICCT 2011, ITST 2012, the IEEE VTC 2013, IWCMC 2015, IWCMC 2016, the IEEE/CIC ICCC 2016, and WPMC 2016.